

# **Folate system correlations in DNA microarray data**

Tomas Radivoyevitch

Department of Epidemiology and Biostatistics

Case Western Reserve University, Cleveland, Ohio 44106 USA

Tel: 216-368-1965; Email: [radivot@hal.cwru.edu](mailto:radivot@hal.cwru.edu)

# Abstract

## Background

Gene expression data is abundantly available from the Gene Expression Omnibus (GEO) and various websites. Pathway specific analyses of gene-gene correlations across these datasets remain relatively unexplored, though they could be informative.

## Methods

Folate gene expression data is explored here in two ways: (1) directly, using gene-gene scatter plots and gene expression time course plots; and (2) indirectly, using de novo purine (DNPS) and thymidylate (DNTS) synthesis flux predictions of a folate model perturbed by relative gene expression modulations of its  $V_{\max}$  parameters.

## Results

Positive correlations within and between the DNPS and DNTS folate cycles are observed in the folate gene expression data. For steady state measurements across childhood leukemia patients, positive correlations between DNPS and DNTS are consistent with higher proliferative fractions requiring higher levels of both fluxes. For cells exposed to ionizing radiation, transient increases in both pathways are consistent with DNA damage driven dNTP demand, and a steadily decreasing backdrop is consistent with radiation induced cell cycle arrest. By and large, folate model based flux predictions paralleled these findings, the main differences being a gain of correlation information for the TEL-AML1 leukemia data, and the loss of one interesting inference, namely, that RNA repair driven DNPS precedes DNA repair driven DNTS after a 10 gray dose of ionizing radiation.

## Conclusions

Pathway focused correlation analyses of DNA microarray data can be informative, with or without a mathematical model. Conceptual models are essential. Mathematical model based analyses should supplement, but should not replace, direct data analyses.

## Background

The folate system (Figure 1A) is central to *de novo* purine synthesis (DNPS) and *de novo* thymidylate synthesis (DNTS) and is a key target of several anti-cancer agents. For example, methotrexate (MTX), in its polyglutamated forms, inhibits dihydrofolate [DHF] reductase (DHFR), thymidylate synthetase (TS), glycinamide ribonucleotide formyltransferase (GART), and other folate system enzymes (see the MTX containing reaction equations [1] in Methods); the novel multi-targeted anti-folate ALIMTA has similar targets [2], though with a very different spectrum of inhibition constants  $K_i$  such that GART inhibition is dominant [3]; the anti-folate raltitrexed (Tomudex) mostly inhibits TS [4]; and 5-fluorouracil also inhibits TS (as FdUMP), though it also kills cells via incorporation into DNA and RNA [5].

Folates convert serine side chains into tetrahydrofolate (THF; Figure 1B) held reactive single-carbons with the following uses: 5-methyl-THF ( $\text{CH}_3\text{THF}$ ) is used to convert homocysteine into methionine; 5,10 methylene-THF ( $\text{CH}_2\text{THF}$ ) is used by TS of DNTS to convert dUMP (deoxyuridylate) into dTMP (thymidylate) for the sole purpose of DNA synthesis, be it scheduled (i.e. DNA replication driven) or unscheduled (i.e. DNA damage driven); and 10-formyl-THF ( $\text{CHOTHF}$ ) is used to set up the purine ring closure reactions of DNPS for many purposes, including the synthesis of RNA, DNA, ATP, GTP and many other molecules, all of which are subject to purine base oxidation and thus replacement after irradiation. These three single-carbon consuming folate functions interact via competition for  $\text{CH}_2\text{THF}$ . Using publicly available DNA microarray data, this study explores folate cycle interactions at the higher level of mRNA. To assess the added value to analyses, of a published mathematical model of the folate system [1], inferences obtained directly from the DNA microarray data are compared here to those obtained indirectly using folate model predictions of DNPS and DNTS based on the same DNA microarray data.

## Methods

### Mathematical model of Morrison and Allegra

The folate cycle model of Morrison and Allegra [1] has the following mathematical form:

$$\begin{aligned} \frac{dDHF^T}{dt} &= \sum_{9,12} r_i - \sum_{10,11} r_i & \frac{dTHF}{dt} &= \sum_{1R,2R,4,6,7,10} r_i - \sum_{1,2,5} r_i & \frac{d(CH_2THF)}{dt} &= \sum_{1,2} r_i - \sum_{1R,2R,3,8,9} r_i \\ \frac{d(CH_3THF)}{dt} &= r_3 - r_4 & \frac{dCHOTHF}{dt} &= \sum_{5,8} r_i - \sum_{6,7} r_i & \frac{dCHODHF}{dt} &= r_{11} - r_{12} \\ \frac{dHCHO}{dt} &= r_{2R} - r_2 & \frac{dFGAR}{dt} &= r_6 - r_{13} & \frac{dAICAR}{dt} &= r_{13} - r_7 - r_{12} \end{aligned}$$

These equations restate the system configuration information of Figure 1A, i.e. they state that the rate at which a metabolite concentration increases equals the sum of the synthesis reaction fluxes (arrows into a node) minus the sum of the degradation reaction fluxes (arrows leaving a node). The  $r_i$  in these equations are:

$$r_1 = V_{SHMT} \cdot \frac{THF / K_{THF}}{1 + THF / K_{THF}} \cdot \frac{Serine / K_{SER}}{1 + Serine / K_{SER}} \quad r_{1R} = V_{SHMTR} \cdot \frac{CH_2THF / K_{CH_2THF}}{1 + CH_2THF / K_{CH_2THF}} \cdot \frac{Glycine / K_{GLY}}{1 + Glycine / K_{GLY}}$$

$$r_2 = h_p \cdot THF \cdot HCHO \quad r_{2R} = h_i \cdot CH_2THF$$

$$r_3 = V_{MTHFR} \cdot \frac{CH_2THF / (K_{CH_2THF} [1 + \sum_{n=1}^5 \frac{x_n}{K_3^{MTX_n}} + \frac{DHF}{K_3^{DHF}}])}{CH_2THF / (K_{CH_2THF} [1 + \sum_{n=1}^5 \frac{x_n}{K_3^{MTX_n}} + \frac{DHF}{K_3^{DHF}}]) + 1} \cdot \frac{NADPH / K_{NADPH}}{1 + NADPH / K_{NADPH}}$$

$$r_4 = V_{MTR} \cdot \frac{CH_2THF / K_{CH_2THF}}{1 + CH_2THF / K_{CH_2THF}} \cdot \frac{Homocysteine / K_{HCYS}}{1 + Homocysteine / K_{HCYS}}$$

$$r_5 = V_{FTS} \cdot \frac{THF / K_{THF}}{1 + THF / K_{THF}} \cdot \frac{ATP / K_{ATP}}{1 + ATP / K_{ATP}} \cdot \frac{Formate / K_{formate}}{1 + Formate / K_{formate}}$$

$$r_6 = V_{GART} \cdot \frac{CHOTHF / (K_{CHOTHF} [1 + \sum_{n=1}^5 \frac{x_n}{K_6^{MTX_n}} + \frac{DHF}{K_6^{DHF}} + \frac{CHODHF}{K_6^{CHODHF}}])}{CHOTHF / (K_{CHOTHF} [1 + \sum_{n=1}^5 \frac{x_n}{K_6^{MTX_n}} + \frac{DHF}{K_6^{DHF}} + \frac{CHODHF}{K_6^{CHODHF}}]) + 1} \cdot \frac{GAR / K_{GAR}}{1 + GAR / K_{GAR}}$$

$$r_7 = V_{ATIC} \cdot \frac{CHOTHF / (K_{CHOTHF} [1 + \sum_{n=1}^5 \frac{x_n}{K_7^{MTX_n}} + \frac{DHF}{K_7^{DHF}} + \frac{CHODHF}{K_7^{CHODHF}}])}{CHOTHF / (K_{CHOTHF} [1 + \sum_{n=1}^5 \frac{x_n}{K_7^{MTX_n}} + \frac{DHF}{K_7^{DHF}} + \frac{CHODHF}{K_7^{CHODHF}}]) + 1} \cdot \frac{AICAR / K_{AICAR}}{1 + AICAR / K_{AICAR}}$$

$$r_8 = V_{MTHFD} \cdot \frac{CH_2THF / K_{CH_2THF}}{1 + CH_2THF / K_{CH_2THF}} \cdot \frac{NADP / K_{NADP}}{1 + NADP / K_{NADP}}$$

$$r_9 = \frac{V_{TS} \frac{dUMP}{K_{dUMP}} \cdot \frac{CH_2THF}{K_{CH_2THF}}}{\left(1 + \sum_2^5 \frac{x_n}{K_9^{MTX_n}} + \frac{DHF}{K_9^{DHF}}\right) + \left(\left(1 + \sum_2^5 \frac{x_n}{K_9^{MTX_n}} + \frac{DHF}{K_9^{DHF}}\right) \left(1 + \frac{CHODHF}{K_9^{CHODHF}} + \frac{CHODHF}{K_9^{CHODHF}} \cdot \frac{x_1}{K_9^{MTX_1}}\right) \frac{dUMP}{K_{dUMP}} + \left(1 + \sum_1^5 \frac{x_n}{K_9^{MTX_n}} + \frac{DHF}{K_9^{DHF}}\right) \frac{dUMP}{K_{dUMP}} \cdot \frac{CH_2THF}{K_{CH_2THF}}\right)}$$

$$r_{10} = k(DHF^T - DHF)$$

$$r_{11} = k_{FDS} \cdot DHF$$

$$r_{12} = V_{ATIC12} \cdot \frac{CHODHF / (K_{CHOTHF} [1 + \sum_1^5 \frac{x_n}{K_7^{MTX_n}} + \frac{DHF}{K_7^{DHF}} + \frac{CHOTHF}{K_{12}^{CHOTHF}}])}{CHODHF / (K_{CHOTHF} [1 + \sum_1^5 \frac{x_n}{K_7^{MTX_n}} + \frac{DHF}{K_7^{DHF}} + \frac{CHOTHF}{K_{12}^{CHOTHF}}]) + 1} \cdot \frac{AICAR / K_{AICAR}}{1 + AICAR / K_{AICAR}}$$

$$r_{13} = V_{FA} \cdot \frac{GLN / K_{GLN}}{1 + GLN / K_{GLN}} \cdot \frac{FGAR / K_{FGAR}}{1 + FGAR / K_{FGAR}}$$

where  $DHF^T - DHF$  (total DHF minus free DHF) is the concentration of DHF bound to DHFR,  $x_i$  is the concentration of  $i$ -glutamated MTX, and all folates are assumed to be penta-glutamated. Not shown are 10 additional differential equations for up to penta-glutamation of MTX either free or bound to DHFR. These 10 equations are irrelevant when  $MTX=0$  as in the microarray data analyses below; they were used here only to validate the current implementation of the model against its previously published responses, see Figure 2 [1].

## Model limitations

Since the model has only one compartment, the cytosol, it cannot handle changes in the mitochondrial enzymes MTHFD2 and SHMT2, nor can it handle changes in the extra-cellular folate hydrolase gene FOLH1 (the gene that codes for prostate-specific membrane antigen, PSMA), so these genes were ignored in the analyses. Further, the folate genes GGH (polyglutamate hydrolase), FPGS (polyglutamate synthase), and RFC (reduced folate carrier), were not considered in the microarray analyses because these reactions are included in the model only for MTX and not folate, and because  $MTX=0$  for the microarray data.

## Model modifications

Flux boundary conditions for dUMP and GAR synthesis in the original model [1] were replaced by downstream concentration boundary conditions set to their initial values. This was done because *steady state* flux differences across patients would otherwise be nullified; e.g. if the flux into GAR were fixed, the steady state flux through GART would also be fixed, and artificially then, there would be no variation in predictions of this flux across patients.

## Model-data linkage

For steady state flux predictions of leukemia patient diagnostic samples, MAS5 microarray measurements of Ross et al [6] and Yeoh et al [7] were normalized by dividing by the mean of the leukemia subtype medians. Step functions from 1 (for  $t < 0$ ) to the resulting metrics (for  $t \geq 0$ ) were then used as modulators of the baseline folate model  $V_{\max}$  values, i.e. microarray data normalization values were equated to the steady state of the model. Individualized patient steady states were then computed as simulation endpoints 40 hours after the  $V_{\max}$  perturbations; all time courses were inspected visually to assure settled steady states at 40 hours. For radiation response data [8], initial measurements were equated to the steady state of the model, so the data was normalized by its values at  $t=0$ . Linear interpolations of the normalized data were then used as time-varying  $V_{\max}$  modulators. For both the steady state leukemia data and the time course radiation response data, proportionality between mRNA levels and protein levels was assumed. This assumption was motivated by simplicity, convenience, and a lack of better alternatives. In the future, as proteomic-transcriptomic combined dynamic response data (e.g. [9]) accrues, this assumption will likely be replaced by a set of gene specific lead-lag filter [10] assumptions. In the meantime, direct proportionality can be viewed and used as a first order approximation, or as a temporary crutch.

## Computational details

The computational environment R [11] was used with R packages of Bioconductor [12] to implement this study. Specifically, the package `Biobase` was used to manipulate microarray data as expression set (class `eset`) objects and `SBMLR` [13, 14] was used to simulate a systems biology markup language (SBML) [15-17] representation of the folate metabolism model [1]. R scripts reproducing figures 2-8 are included with `SBMLR` as an illustrative example of package use. For convenience, array data used in this study have been repackaged as `eset` objects in R data packages available from the author's website [14]. Throughout, genes with multiple probe sets were represented by the set with the highest average value.

## Results

### Folate system correlations across childhood leukemias

Childhood acute lymphoblastic leukemia (ALL) microarray data of Ross et al [6] and Yeoh et al [7] is shown in Figures 3 and 4. Several points can be made regarding this steady state diagnostic bone marrow data. Firstly, since `TYMS` and `DHFR` (similarly `MTHFD1`, `GART` and `ATIC`) operate in series, it makes sense that the system would attempt to match these throughput capabilities as closely as possible to avoid the costs of maintaining unneeded excess "equipment." Thus, positive correlations *within* the DNPS and DNTS branches are expected. Secondly, growing cells require commensurate increases in both DNTS and DNPS, so positive correlations *between* these cycles are also expected. Finally, DNPS genes are higher in T cell leukemic cells than in B-cell leukemic cells, consistent with measured DNPS fluxes being three fold higher in T cells than in B cells [18].

To assess the added value of the folate model, since `MTHFD1` and `TYMS` are the gatekeepers of DNPS and DNTS, respectively, correlation plots for these genes were compared to corresponding flux predictions in Figure 5. The plots show that, for the most

part, model predicted fluxes are more correlated than measured MTHFD1 vs. TYMS mRNA. To estimate the amount of correlation attributable to steady state flux constraints alone, 1000 uncorrelated normally distributed ( $\mu = 1$ ;  $\sigma = 0.30$ ) random numbers were applied to the model as  $V_{\max}$  modulators. The amount of correlation ( $r=0.18$ , Figure 6) is more than that induced by the model (beyond gatekeeper correlations) for BCR-ABL and T cell leukemias (Figure 5), but less than induced for TEL-AML1 leukemias. Thus, for TEL-AML leukemias additional information must have been contributed by the other folate genes inputted into the model, suggesting more folate system coordination in this more curable leukemia subtype.

### **Folate system analysis of radiation time course data**

Folate system correlations in radiation response time course data [8] were also investigated. The data (Fig. 7) shows that TS, DHFR, GARFT and MTHFD each have a dose-dependent transient increase after irradiation, consistent with radiation induced DNA damage causing a transient rise and fall in P53 activity [19] with subsequent induction of ribonucleotide reductase subunit P53R2 [20] causing a transient increase in *de novo* deoxynucleotide synthesis for DNA repair; a 17-fold increase in R2 protein 24 h after irradiation [21] is radioprotective [22], further supporting this conjecture. The data also shows a steady decline in many of the gene expression time courses, possibly due to radiation induced cell cycle arrest. At 10 gray, inspection of TS, DHFR, GARFT and MTHFD further suggests that RNA repair driven DNPS (peak at 2 hours) precedes DNA repair driven DNTS (peak at 6 hours).

In Figure 7, gene expression time courses are more likely to be signals if they differ between 3 and 10 gray only in terms of minor time shifts and dose ordered amplitude changes. Based on this, MTHFR and SHMT1 were dismissed as being noise. The remaining six gene expression time courses were normalized by their values at  $t=0$  and applied to the folate

model as linearly interpolated time-varying modulators of corresponding  $V_{\max}$  parameters. The resulting model-based predicted time courses are shown in Figure 8. These plots affirm the “dose-dependent spike resting on a decreasing backdrop” response of DNPS and DNTS that was qualitatively inferred from Figure 7. In contrast to the data itself, however, at 10 gray, RNA repair driven DNPS (peak at 12 hours) and DNA repair driven DNTS (peak at 10 hours) are reverse ordered and delayed. Since NTP production tends to be in high gear full time, compared to dNTP production, it likely has a greater ability to respond rapidly to oxidative damage. Further, a dNTP synthesis flux peak at 6 hours compared to 10 hours is more consistent with a P53 spike at 5 hours [19]. Thus, until measurements of DNPS and DNTS in 10 gray irradiated cells suggest otherwise, the direct data inference that RNA repair precedes DNA repair is tentatively more credible than its model-based counterpart.

## Discussion

Pathway focused analyses are essential for gene-gene correlation studies because the number of possible correlations would otherwise be too large to investigate. For example, if a chip carries 10,000 genes, the number of 2D plots requiring correlation tests is then 10,000 choose 2, or ~50 million, i.e. a serious problem that is not encountered in pathway focused studies.

Although TS and DHFR are predominantly controlled at the protein level, Figures 3, 4 and 7 indicate that some control effort is also exerted at the mRNA level. Thus, protein level control may dominate a particular regulatory system, but mRNA signals may still be informative of what the overall system is trying to accomplish. That DNPS and DNTS are correlated in a consistent manner across disparate steady state and transient datasets lends credence to the view that DNA microarray data is a valid source of biochemical system coordination and control information. The prospect of characterizing cancers by losses in coordination in various biochemical systems is certainly intriguing.

## Conclusions

The main conclusion of this paper is that interesting inferences can be gleaned from genome-wide microarray data (with or without mathematical models) if gene-gene correlations are analyzed in a pathway specific manner. The added value of analyzing microarray data using Morrison and Allegra's folate model, relative to simply *eye-balling* the gene expression data, was minimal. For example, in Figure 5, save the ability of the model to identify TEL-AML1 leukemias as different, gate-keeper focused gene expression scatter plots are almost as revealing as model-predicted DNPS vs. DNTS scatter plots. Similarly, for the radiation time course data in Figures 7 and 8, the spike increase in DNPS and DNTS and the baseline downward trend at larger times are apparent using either approach.

This study used: a) conceptual models of the functional roles of folates and of the biological effects of ionizing radiation, to guide, focus, validate and discriminate inferences; and b) knowledge of genes and system scope to reduce the multivariate analysis to a manageable dimension correlated subspace. Pathway focused analyses can therefore be expected to work best when the biochemical system and the experimental data conditions are well understood.

To go beyond qualitative statements and to actually plot predictions (Figures 5 and 8), quantitative models are needed. Further, as pathway knowledge expands in scope and complexity, *gedanken* experiments underlying *eye-ball* data analyses will become increasingly difficult to carry out, and mathematical models will then become indispensable. If metabolic flux constraints are consonant with mRNA level control system objectives, models may also find uses as quantifiers of gene expression coordination losses in cancer (Figures 5 and 6). Thus, model-based approaches must continue to be developed. The lost inference that RNA repair precedes DNA repair suggests that model-based approaches should supplement, but should not replace, direct data analyses.

## Competing interests

TR has no competing interests

## List of abbreviations

DHF = dihydrofolate; THF = tetrahydrofolate; DNPS = de novo purine synthesis; DNTS = de novo thymidylate synthesis; DHFR = DHF reductase; TS = thymidylate synthetase (protein); TYMS = thymidylate synthetase (gene); MTHFR = methylene-THF reductase; MTR = methyl-THF transferase; FTS = formyl-THF synthetase; FDS = formyl-DHF synthetase; SHMT = serine hydroxy methyl transferase; GAR = glycinamide ribonucleotide; FGAR = formyl-GAR; GART = GAR formyltransferase; AICAR = aminoimidazole-4-carboxamide ribonucleotide; FAICAR = formyl-AICAR; dUMP = deoxyuridylate; dTMP = thymidylate; MTX = methotrexate; SBML = Systems Biology Markup Language.

## Authors' contributions

TR is the sole contributor.

## Acknowledgements

This work was supported by the Comprehensive Cancer Center of Case Western Reserve University and University Hospitals of Cleveland (P30 CA43703), the American Cancer Society (IRG-91-022-09), the National Cancer Institute's Integrative Cancer Biology Program (P20 CA112963-01) and NIH grant 1K25 CA104791-01A1.

## References

1. Morrison PF, Allegra CJ: **Folate cycle kinetics in human breast cancer cells.** *JBiolChem* 1989, **264**:10552-10566.
2. Curtin NJ, Hughes AN: **Pemetrexed disodium, a novel antifolate with multiple targets.** *Lancet Oncol* 2001, **2**:298-306.
3. Shih C, Habeck LL, Mendelsohn LG, Chen VJ, Schultz RM: **Multiple folate enzyme inhibition: mechanism of a novel pyrrolopyrimidine-based antifolate LY231514 (MTA).** *Adv Enzyme Regul* 1998, **38**:135-152.
4. Yin MB, Guimaraes MA, Zhang ZG, Arredondo MA, Rustum YM: **Time dependence of DNA lesions and growth inhibition by ICI D1694, a new**

- quinazoline antifolate thymidylate synthase inhibitor.** *Cancer Res* 1992, **52**:5900-5905.
5. Spiegelman S, Sawyer R, Nayak R, Ritzi E, Stolfi R, Martin D: **Improving the anti-tumor activity of 5-fluorouracil by increasing its incorporation into RNA via metabolic modulation.** *Proc Natl Acad Sci USA* 1980, **77**:4966-4970.
  6. Ross ME, Zhou X, Song G, Shurtleff SA, Girtman K, Williams WK, Liu HC, Mahfouz R, Raimondi SC, Lenny N, et al: **Classification of pediatric acute lymphoblastic leukemia by gene expression profiling.** *Blood* 2003, **102**:2951-2959.
  7. Yeoh EJ, Ross ME, Shurtleff SA, Williams WK, Patel D, Mahfouz R, Behm FG, Raimondi SC, Relling MV, Patel A, et al: **Classification, subtype discovery, and prediction of outcome in pediatric acute lymphoblastic leukemia by gene expression profiling.** *Cancer Cell* 2002, **1**:133-143.
  8. Jen KY, Cheung VG: **Transcriptional response of lymphoblastoid cells to ionizing radiation.** *Genome Res* 2003, **13**:2092-2100.
  9. Zheng PZ, Wang KK, Zhang QY, Huang QH, Du YZ, Zhang QH, Xiao DK, Shen SH, Imbeaud S, Eveno E, et al: **Systems analysis of transcriptome and proteome in retinoic acid/arsenic trioxide-induced cell differentiation/apoptosis of promyelocytic leukemia.** *Proc Natl Acad Sci U S A* 2005.
  10. Oppenheim AV, Willsky AS, Young IT: *Signals and Systems*. Prentice Hall, Englewood Cliffs, NJ; 1983.
  11. Ihaka R, Gentleman R: **R: a language for data analysis and graphics.** *Journal of Computational and graphical statistics* 1996, **5**:299-314.
  12. Gentleman RC, Carey VJ, Bates DM, Bolstad B, Dettling M, Dudoit S, Ellis B, Gautier L, Ge Y, Gentry J, et al: **Bioconductor: open software development for computational biology and bioinformatics.** *Genome Biol* 2004, **5**:R80.
  13. **SBMLR** [<http://www.bioconductor.org/repository/devel/package/html/SBMLR.html>]
  14. **Radivoyevitch Lab** [<http://epbi-radivot.cwru.edu/>]
  15. **Systems Biology Markup Language** [<http://sbml.org>]
  16. Hucka M, Finney A, Sauro HM, Bolouri H, Doyle JC, Kitano H, Arkin AP, Bornstein BJ, Bray D, Cornish-Bowden A, et al: **The systems biology markup language (SBML): a medium for representation and exchange of biochemical network models.** *Bioinformatics* 2003, **19**:524-531.
  17. Finney A, Hucka M: **Systems biology markup language: Level 2 and beyond.** *Biochem Soc Trans* 2003, **31**:1472-1473.
  18. Dervieux T, Brenner TL, Hon YY, Zhou Y, Hancock ML, Sandlund JT, Rivera GK, Ribeiro RC, Boyett JM, Pui CH, et al: **De novo purine synthesis inhibition and antileukemic effects of mercaptopurine alone or in combination with methotrexate in vivo.** *Blood* 2002, **100**:1240-1247.
  19. Lahav G, Rosenfeld N, Sigal A, Geva-Zatorsky N, Levine AJ, Elowitz MB, Alon U: **Dynamics of the p53-Mdm2 feedback loop in individual cells.** *Nat Genet* 2004, **36**:147-150.
  20. Tanaka H, Arakawa H, Yamaguchi T, Shiraishi K, Fukuda S, Matsui K, Takei Y, Nakamura Y: **A ribonucleotide reductase gene involved in a p53-dependent cell-cycle checkpoint for DNA damage.** *Nature* 2000, **404**:42-49.
  21. Kuo ML, Kinsella TJ: **Expression of ribonucleotide reductase after ionizing radiation in human cervical carcinoma cells.** *Cancer Res* 1998, **58**:2245-2252.
  22. Kuo ML, Hwang HS, Sosnay PR, Kunugi KA, Kinsella TJ: **Overexpression of the R2 subunit of ribonucleotide reductase in human nasopharyngeal cancer cells reduces radiosensitivity.** *Cancer J* 2003, **9**:277-285.

## Figures

**Figure 1.** The folate cycle model of Morrison and Allegra [1] (A) and the molecular structure of folate (B).

**Figure 2.** Morrison and Allegra's model [1] responding to 1  $\mu\text{M}$  MTX applied continuously after  $t=0$ . Concentrations are in  $\mu\text{M}$  (top 6 plots) and fluxes are in  $\mu\text{M}/\text{hour}$  (bottom 3 plots).

**Figure 3.** MAS5 U133a folate gene expression data of Ross et al [7]. Symbols are TEL-AML1 (B), BCR-ABL (b) and T-cell (T). In mirrored positions relative to the main diagonal, corresponding Pearson correlation coefficients  $r$  are given with their P values.

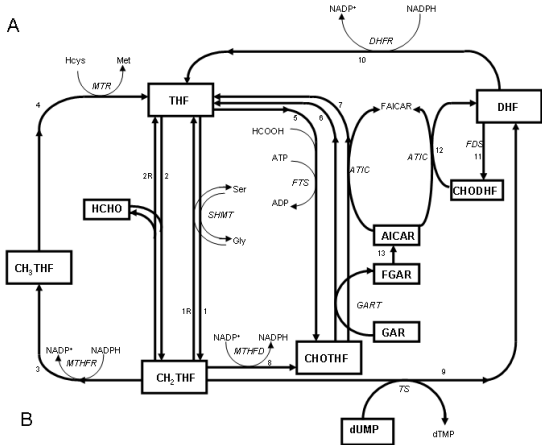
**Figure 4.** MAS5 U95av2 folate gene expression data of Yeoh et al [8]. Only the Yeoh et al [8] patients who are also in the Ross et al dataset [7] are considered. MAS5 summary measures were computed from cel files using Bioconductor's AFFY package. Symbols are as in Figure 3.

**Figure 5.** Comparisons of measured MTHFD1 vs. TYMS versus predicted DNPS vs. DNTS.

**Figure 6.** DNPS vs. DNTS predicted with random numbers replacing Figures 3 & 4.

**Figure 7.** Lymphocyte radiation response data of Jen and Cheung [8]. SHMT1 and MTHFR were not applied to the folate model, see text. Time is in hours.

**Figure 8.** The folate model's response to the radiation time course data. Fluxes are in  $\mu\text{M}/\text{hr}$ .



**B**

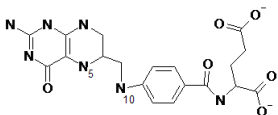


Figure 1

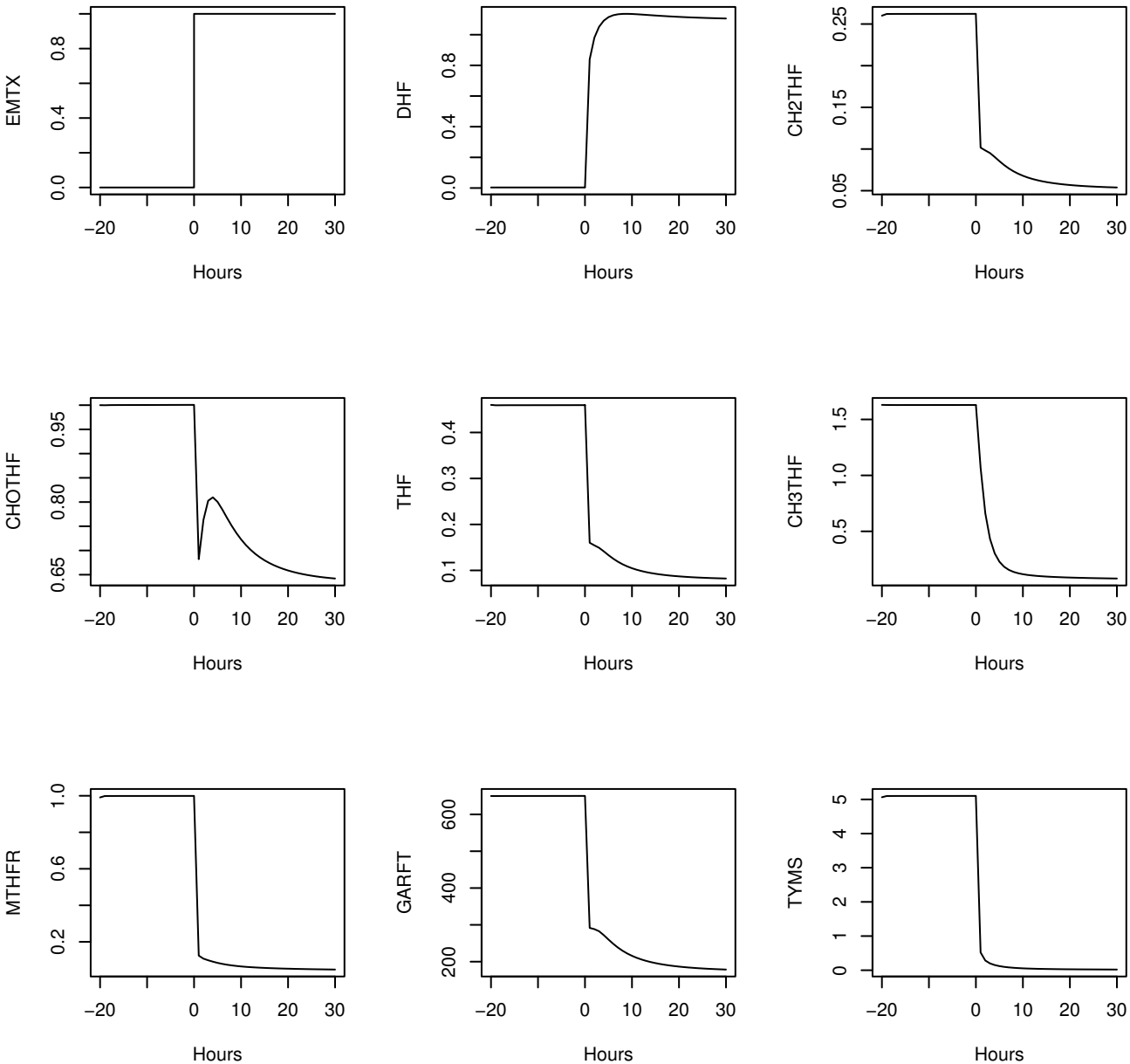


Figure 2

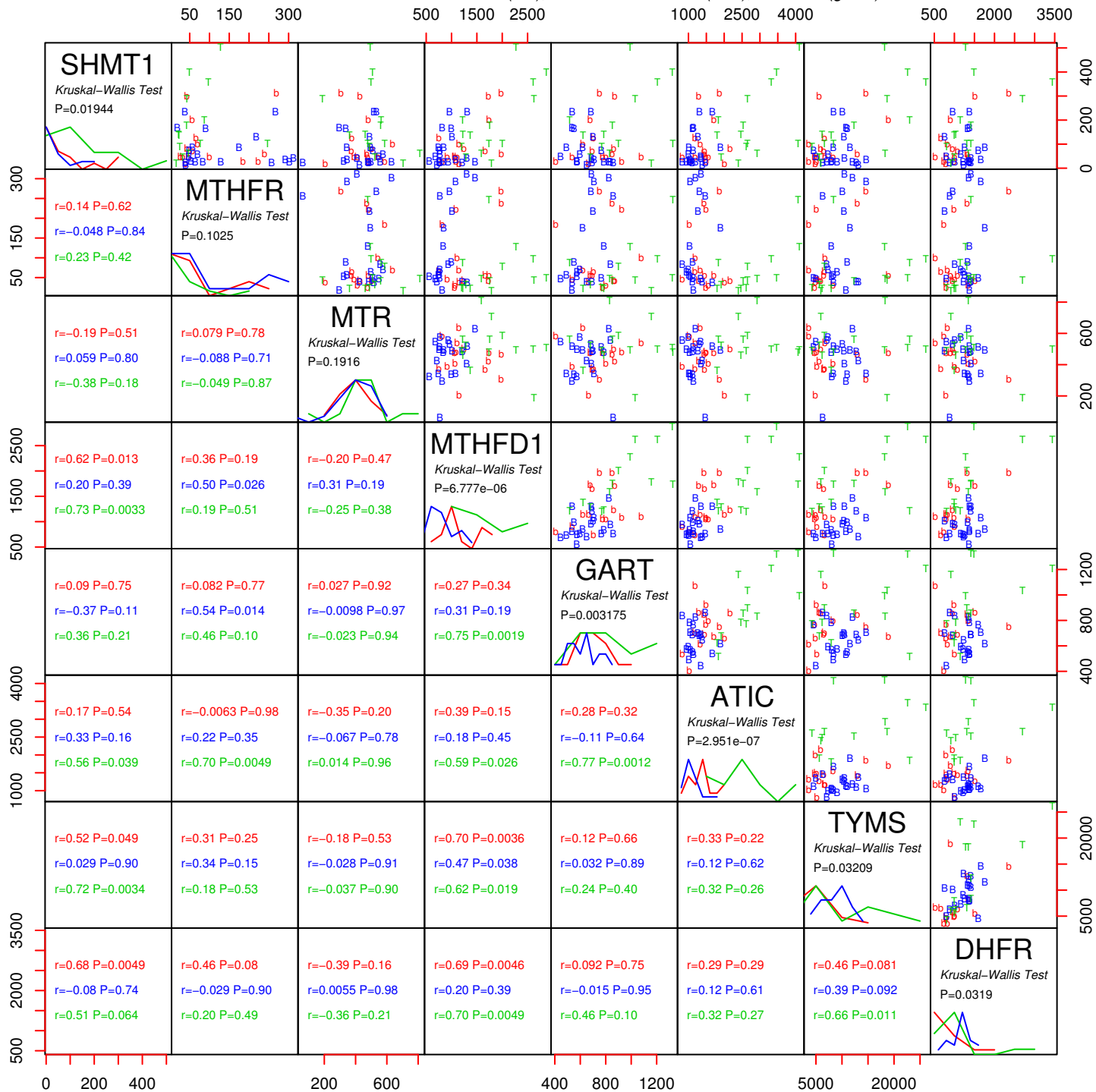


Figure 3

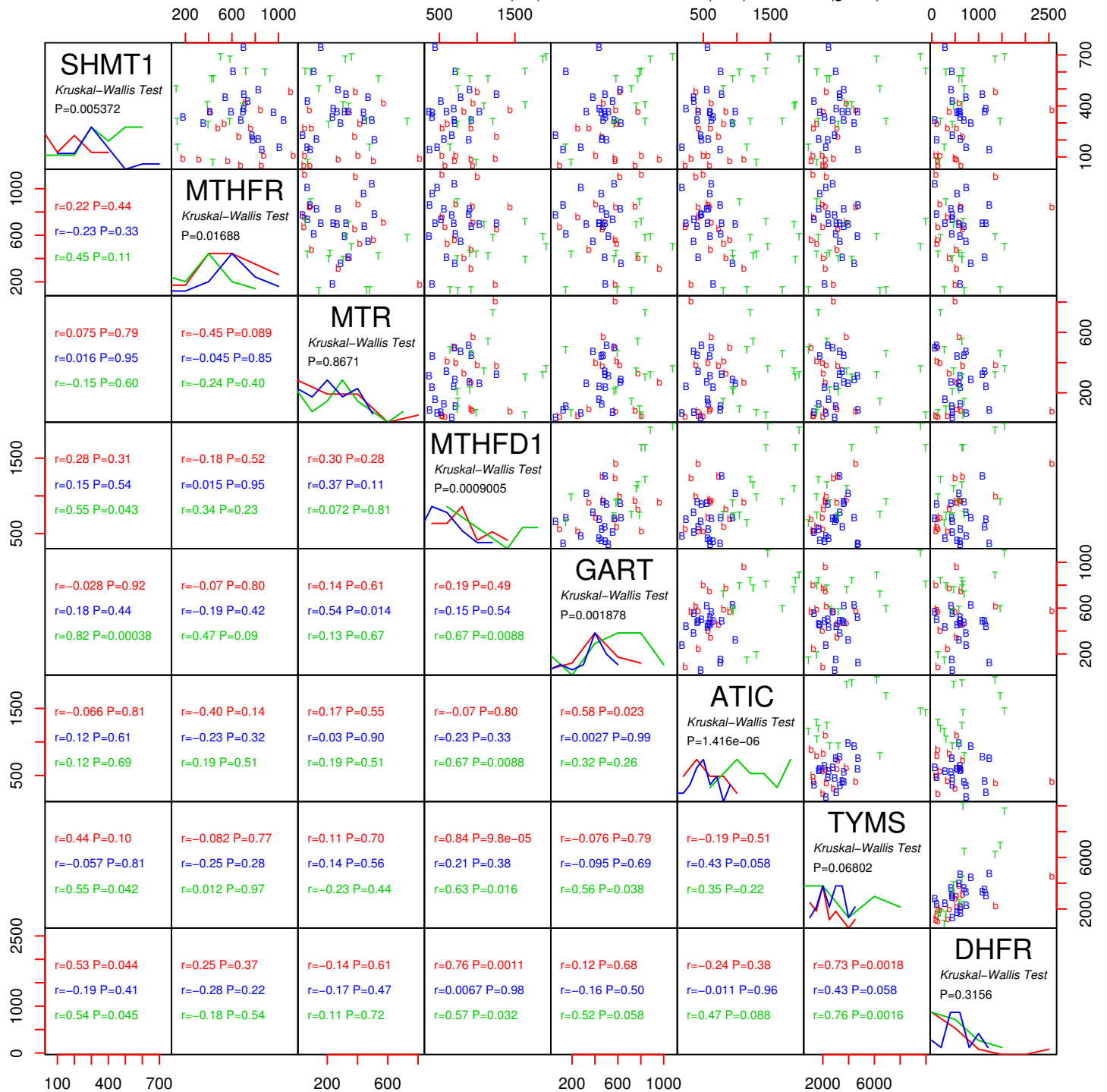
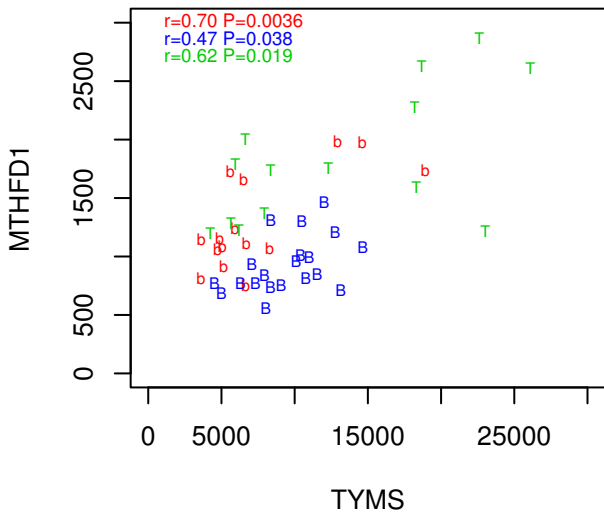
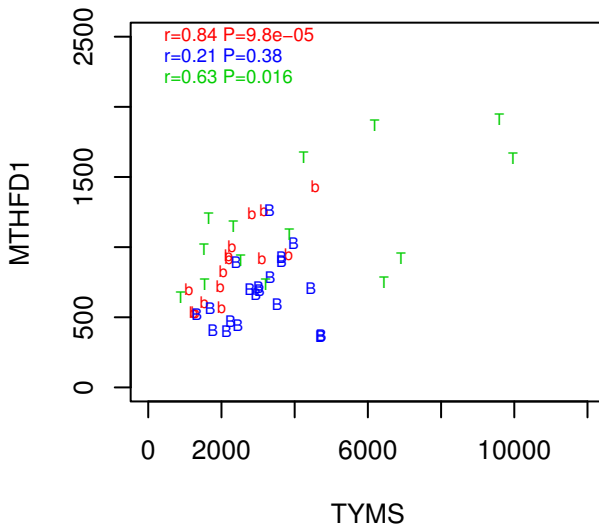


Figure 4

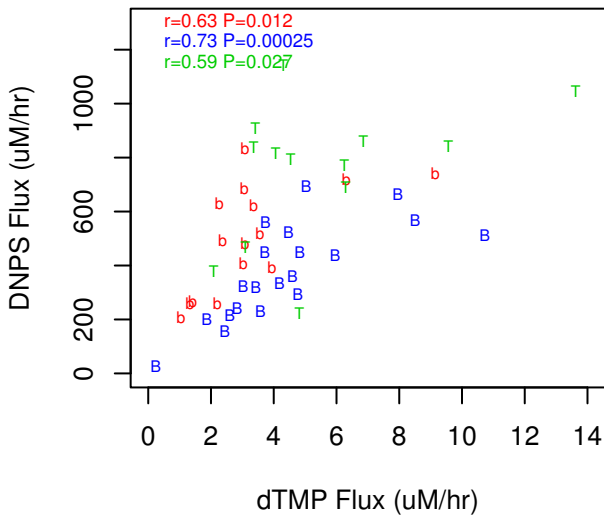
Ross et al.



Yeoh et al.



Ross et al.



Yeoh et al.

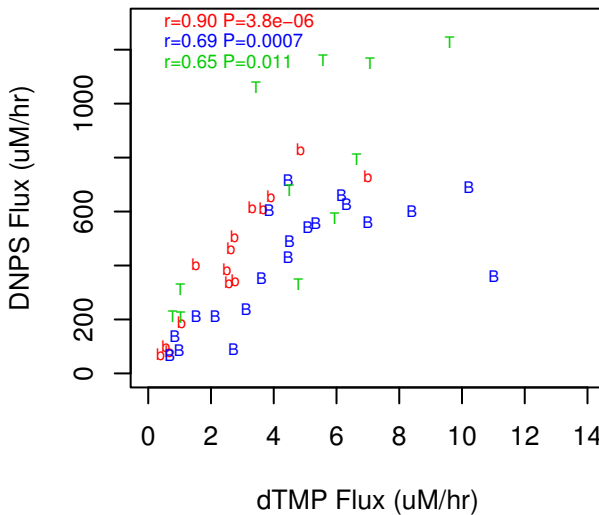


Figure 5

*Random*

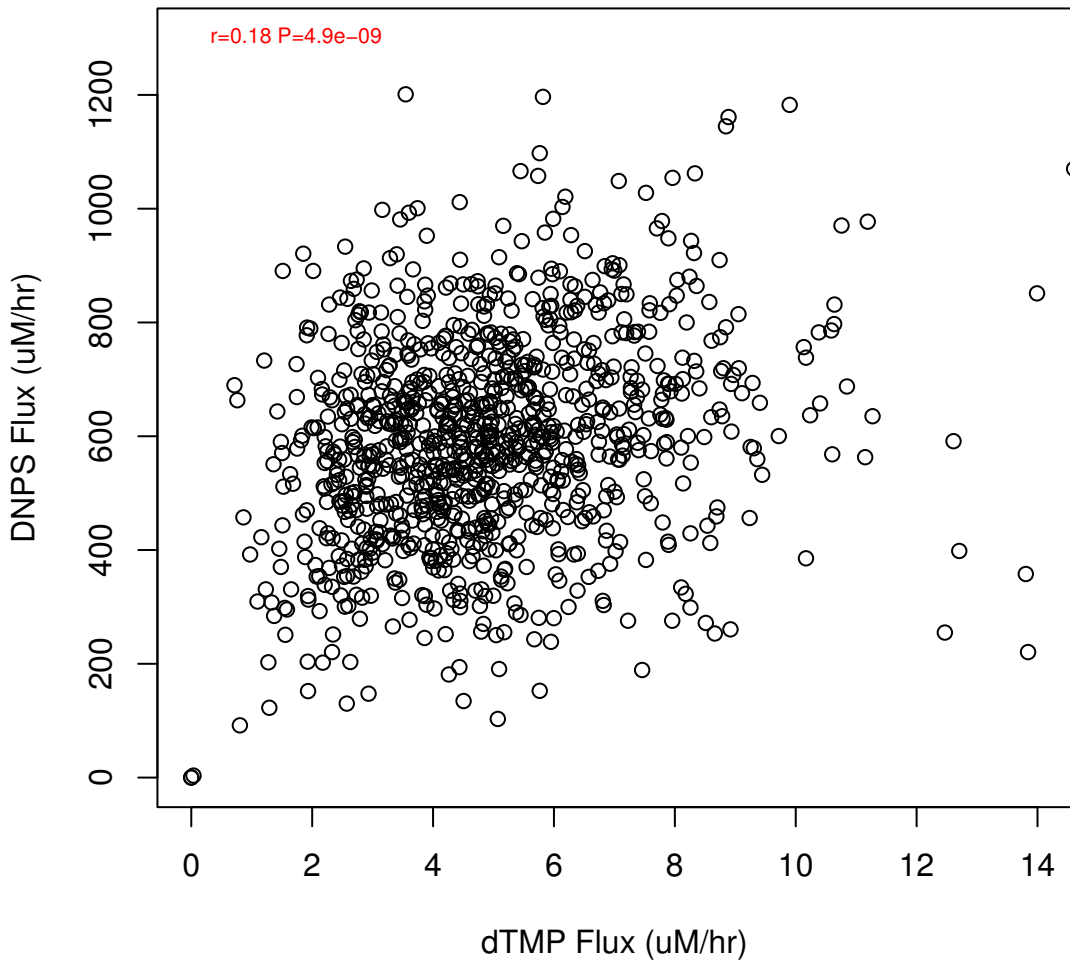


Figure 6

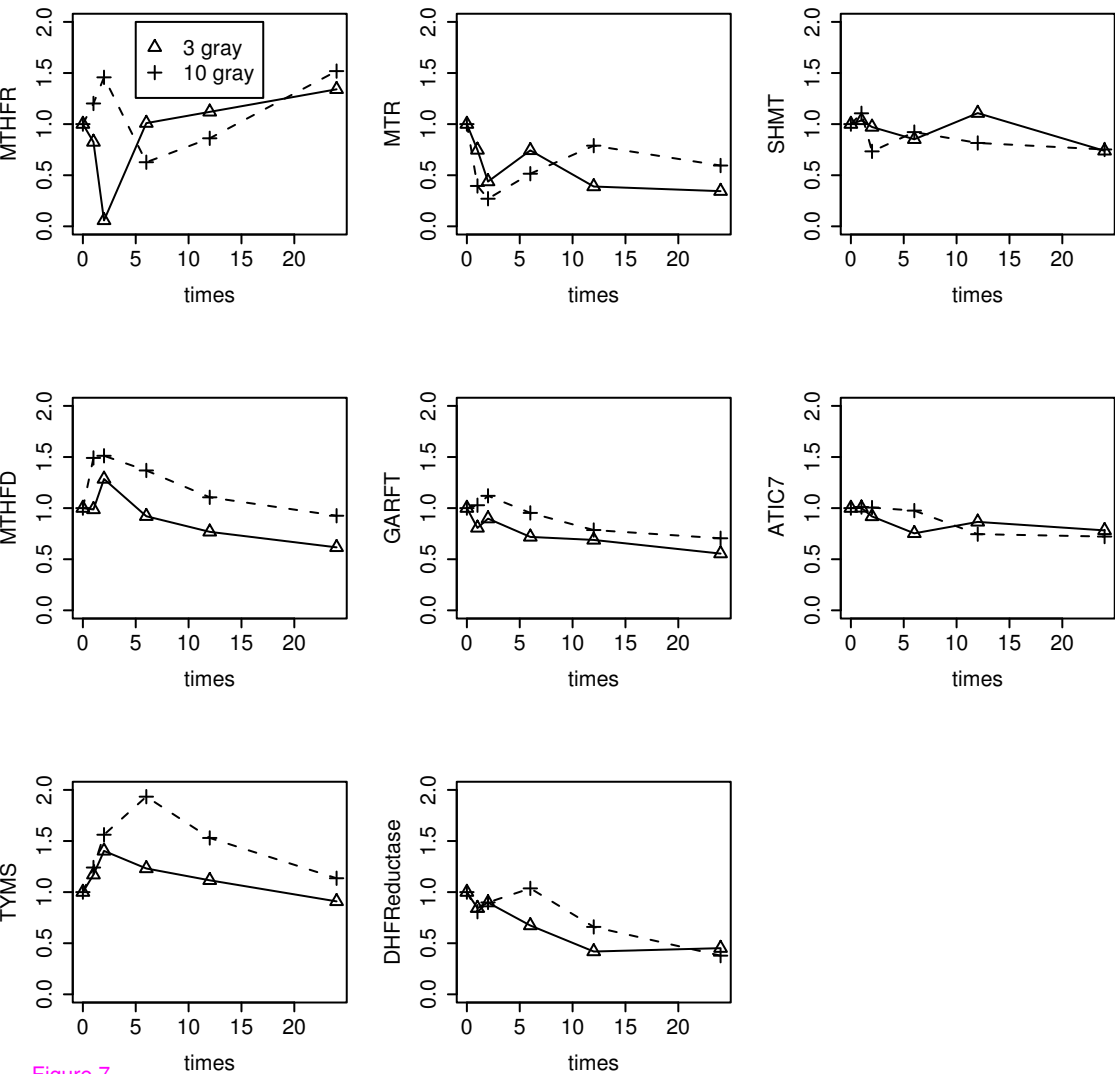


Figure 7

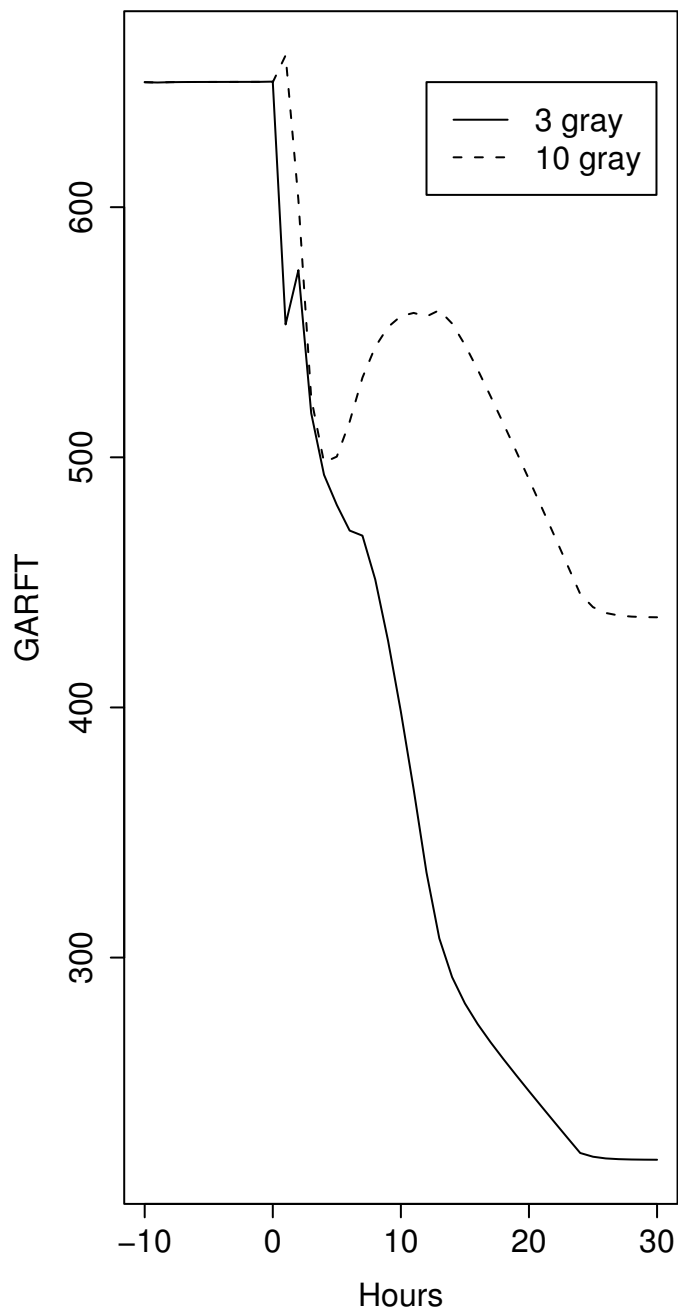
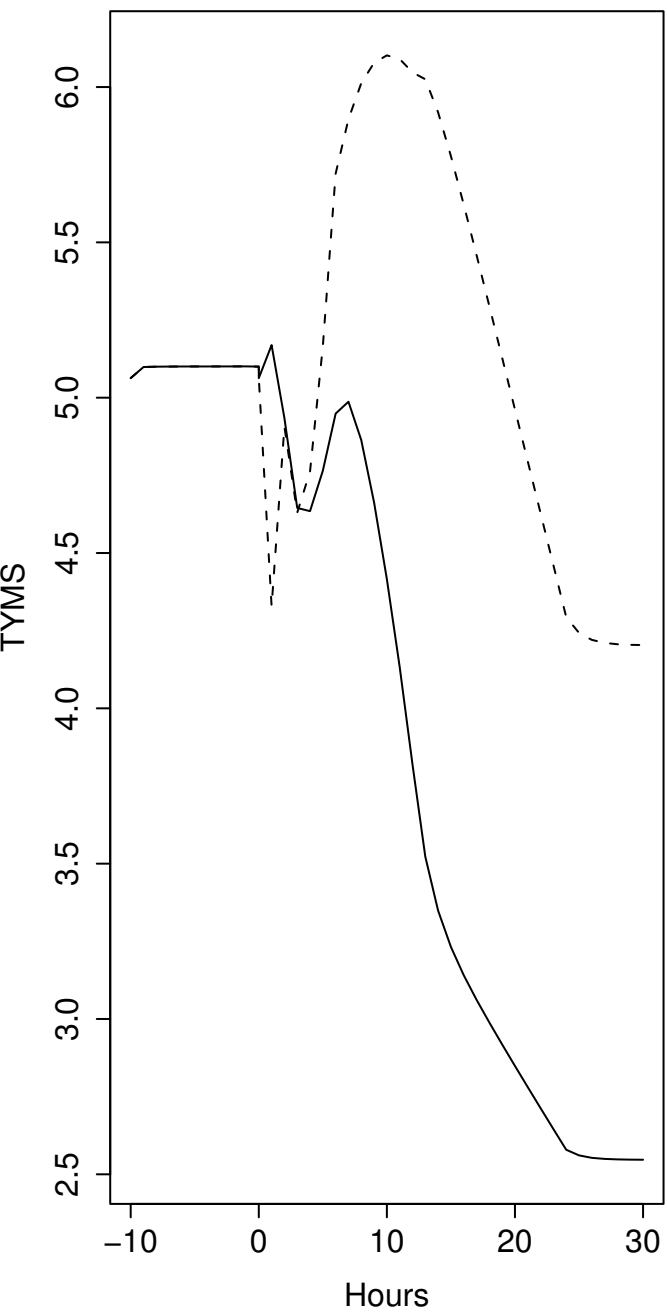


Figure 8